[Article] DOI: 10.13208/j.electrochem.2214003 Http://electrochem.xmu.edu.cn

Self-Supporting NiFe LDHs@Co-OH-CO_3 Nanorod Array Electrode for Alkaline Anion Exchange Membrane Water Electrolyzer

Dan-Dan Guo[1,2], Hong-Mei Yu[1*], Jun Chi[1], Zhi-Gang Shao[1*]

(*1. Fuel Cell System and Engineering Laboratory, Key Laboratory of Fuel Cells & Hybrid Power Sources, Dalian Institute of Chemical Physics, Chinese Academy of Sciences, Dalian 116023, China;*
2. University of Chinese Academy of Sciences, Beijing, 100049, China)

Abstract: The development of efficient and durable electrodes for anion exchange membrane water electrolyzers (AEMWEs) is essential for hydrogen production. In this work, 2D NiFe layered double hydroxides (NiFe LDHs) nanosheets were grown on the 1D cobaltous carbonate hydroxide nanowires array (Co-OH-CO_3) and the unique 3D layered self-supporting nanorod array (NiFe LDHs@Co-OH-CO_3/NF) electrode was obtained. Importantly, we demonstrated an efficient and durable self-supporting NiFe LDHs@Co-OH-CO_3/NF electrode for oxygen evolution reaction (OER) and as the anode of the AEMWE. In a three-electrode system, the self-supporting NiFe LDHs@Co-OH-CO_3/NF electrode showed excellent catalytic activity for OER, with an overpotential of 215 mV at a current density of 20 mA·cm^{-2} in 1 mol·L^{-1} KOH , and the promising AEMWE performance upon using as the anode, with a current density of 0.5 A·cm^{-2} at 1.72 V in 1 mol·L^{-1} KOH at 70 °C. The experimental results further revealed the outstanding performance of the electrode with the special morphological structure. The 3D layered structure of nanorod array electrode could effectively prevent the agglomeration of nanosheets, which is conducive to electron transfer and provides a large number of edge active sites for water electrolyzer.

Key words: NiFe layered double hydroxides; oxygen evolution reaction; anion exchange membrane water electrolyzer

1 Introduction

Hydrogen is a clean energy carrier with the advantages of high energy density, clean and pollution-free, which is considered as a "green" energy carrier[1]. Among many hydrogen production methods, water electrolysis has become the most potential "green" hydrogen production method due to its advantages of the environment-friendly process, high product purity, and zero carbon emission[2]. The water electrolysis process involves two half-reactions: hydrogen evolution reaction (HER) and oxygen evolution reaction (OER)[3, 4]. Compared with HER, the OER involves a complex multi-electron transfer process, which is essentially slow in reaction kinetics and generally has low electrocatalytic activity, leading to low efficiency in energy conversion[5, 6].

To improve the efficiency of alkaline AEMWEs, it is very important to construct active materials with significantly enhanced OER performance[7]. Due to the strong acid and high oxidation potential of the proton exchange membrane (PEM) water electrolysis system[8], traditional non-noble metal catalysts are unstable under such operating conditions and can hardly meet the requirement of long-term stable operation. Ir-based[9] and Ru-based[10] catalysts are still recognized as the best OER catalyst, but their high cost

Cite as: Guo D D, Yu H M, Chi J, Shao Z G. Self-supporting NiFe LDHs@Co-OH-CO_3 nanorod array electrode for alkaline anion exchange membrane water electrolyzer. *J. Electrochem.*, 2022, 28(9): 2214003.

Received: 2022-05-23, Revised: 2022-06-10. *Corresponding author, Tel: (86-411)84379051, E-mail: hmyu@dicp.ac.cn; Tel: (86-411) 84379153, zhgshao@dicp.ac.cn

and scarce shortage restrict their widespread application[1, 11, 12]. Therefore, it is of great significance to develop OER electrocatalysts based on non-noble metals (Fe, Co, Ni, Mo, and Cu) with good catalytic activity, high stability, and low cost in an alkaline system[1, 13].

In alkaline conditions, NiFe-based bimetallic compounds, such as NiFe LDHs[14], NiFe-based metal-organic frameworks[15, 16], NiFe-based (oxygen) hydroxides or NiFe-based oxides[17-19], NiFe alloys[20], and NiFe-based non-oxides[21], have been studied for OER electrocatalysts due to their low cost and abundant resources[22]. Among them, NiFe-based layered double hydroxides have shown better activity than other transition-metal compounds due to their unique electronic structure, appropriate electronic configuration, rich valence states, and diverse compositions[23, 24]. Various strategies have been developed to improve the performance of NiFe-based OER electrocatalysts. For example, the NiFe-based nanomaterials combined with GO or CNT and metal substrates could enhance the conductivity[14, 25].

Recently, the self-supporting NiFe LDHs-based electrodes have been studied in alkaline water electrolysis[3, 26]. Chi et al.[27] prepared the self-supporting VA FeOOH/NiFe LDHs-NF OER electrode with the overpotential of 208 mV at the current density of 10 mA·cm^{-2}. Zhu et al.[2] prepared the self-supporting Cr1/FeNi-LDH-SS OER electrode with the overpotential of 202 mV at the current density of 10 mA·cm^{-2}. Jiao et al.[28] studied the self-supporting CoP@NiFe-OH/SPNF OER electrode with the overpotential of 220 mV at the current density of 20 mA·cm^{-2}. These nanomaterials were directly grown on the conductive substrates (such as nickel foam, copper foam, and stainless steel mesh) without using the binder, which can effectively improve the conductivity and stability of the materials. Moreover, the 2D NiFe LDHs nanosheet materials have the edge site coordination and can expose a large number of active sites, which can provide rich active sites. However, the pure 2D NiFe LDHs nanosheets are prone to stacking in the process of synthesis, which will reduce the exposure of active sites and catalytic efficiency. Efforts have been made to develop an effective strategy to optimize the performance of the electrodes[29, 30]. Studies have proved that the effective methods to optimize the OER catalytic activity of NiFe-based LDHs were electronic structure modification and morphological control[30-32]. Therefore, it is of great significance to design a 3D layered NiFe-based nanorod array OER electrode to enhance catalytic activity and stability.

Here, we synthesized the 3D layered ordered nanorod array as the self-supporting NiFe LDHs@Co-OH-CO_3/NF electrode for both the alkaline water electrolyzer OER electrode and the AEMWE anode electrode. In particular, the inner layer of Co-OH-CO_3 can effectively prevent the agglomeration of NiFe LDHs nanosheets, which is conducive to electron transfer and provides a large number of edge and interface sites for water electrolyzer. The outer layer of NiFe LDHs nanosheets crosses each other to form rich and regular pores, which not only can significantly increase the catalytic active sites, but also can reduce the ion diffusion distance and transmission resistance. As a result, the optimized NiFe LDHs@Co-OH-CO_3/NF electrode showed a low overpotential of 215 mV at a current density of 20 mA·cm^{-2}. In addition, the electrode was used as the anode of AEMWE, with the current density of 0.5 A·cm^{-2} and the cell voltage of 1.72 V. This is attributed to the unique morphology of the electrode, which not only provides more active sites, but also is conducive to electrolyte penetration and gas release during the catalytic reaction process.

2 Experimental

2.1 Chemicals and Materials

Nickel foam (NF, Ni ⩾ 99.9%, thickness of 1 mm) was purchased from Lizhiyuan Co., Ltd (Shanxi China). Cobalt nitrate hexahydrate ($Co(NO)_3 \cdot 6H_2O$, ⩾ 99.99%), nickel nitrate hexahydrate ($Ni(NO)_3 \cdot 6H_2O$, ⩾ 98%), ammonium fluoride (NH_4F, ⩾ 98%), urea ($(NH_2)_2CO$, ⩾ 98%), boracic acid (H_3BO_3, ⩾ 98%), ammonium oxalate ($(NH_4)_2C_2O_4$, ⩾ 98%) and potassium hydroxide (KOH, ⩾ 99.99%) were purchased from Shanghai Aladdin. Ferrous chloride

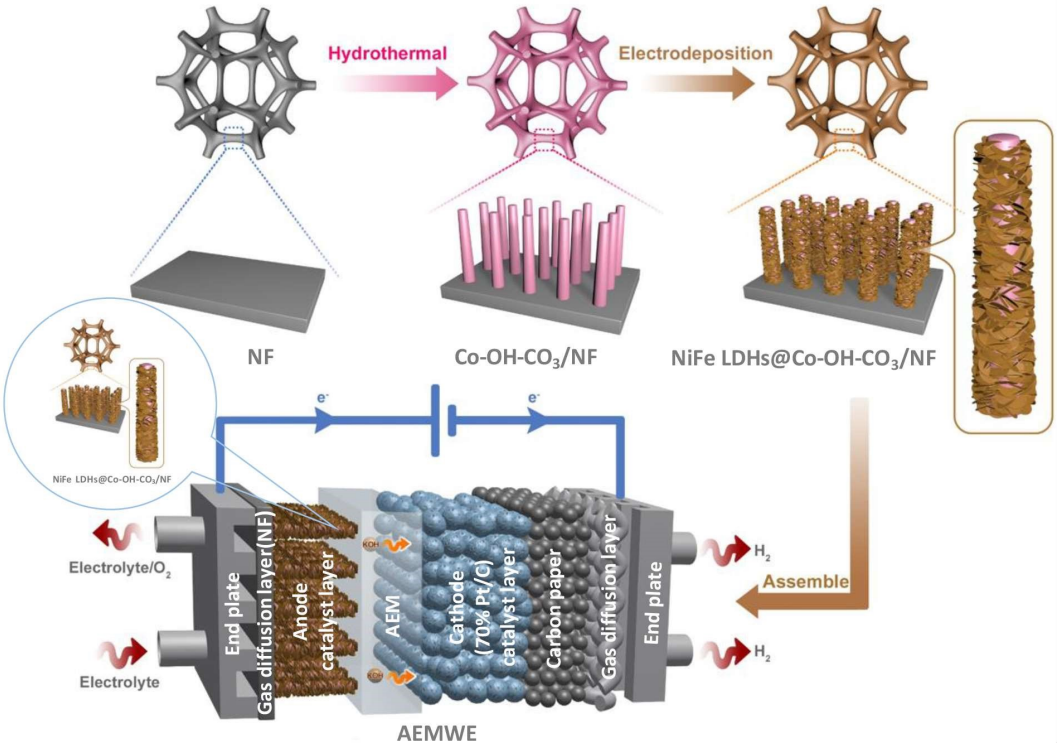

Figure 1 Schematic preparations of NiFe LDHs@Co-OH-CO_3/NF and AEMWE single-cell. (color on line)

($FeCl_2 \cdot 4H_2O$, ≥ 98%), absolute alcohol, acetone (C_3H_6O), and hydrochloric acid (HCl, 36% ~ 38%) were purchased from Damao Co., Ltd. Pt/C (70wt%) was purchased from Johnson Matthey. All chemicals were used as received without any further purification. Millipore water was used in all experiments.

2.2 Catalyst Preparations

2.2.1 Preparation of Co-OH-CO_3/NF

First, the NF (2 cm × 5 cm) was cleaned in acetone solution, 3 mol·L^{-1} HCl, absolute alcohol, and deionized water to remove the nickel oxides on the surface. In a typical procedure, $Co(NO)_3 \cdot 6H_2O$ (1.176 g) and NH_4F (0.148 g) were added into 30 mL deionized water and stirred for 10 min, then $CO(NH_2)_2$ (0.485 g) was dissolved in 42 mL deionized water and stirred for 10 min; The two parts of the solution were mixed and stirred for 30 min to complete the precursor solution. Subsequently, the precursor solution was transferred to the 100 mL Teflon-liner stainless steel autoclave, and the NF was vertically immersed in the precursor solution. The sealed autoclave was maintained at 120 ℃ for 5 h. After the reaction was finished and cooled to room temperature, the obtained self-supporting cobaltous carbonate hydroxide nanowires array electrode was washed with abundant distilled water and dried for next experiment use. The self-supporting cobaltous carbonate hydroxide nanowires array electrode was denoted as Co-OH-CO_3/NF.

2.2.2 Preparation of NiFe LDHs@Co-OH-CO_3/NF

Since the Co-OH-CO_3/NF electrode has a low overpotential of 295 mV at a current density of 20 mA·cm^{-2}. Therefore, it is necessary to further optimize the structure and morphology of the Co-OH-CO_3/NF electrode to improve OER activity. In a typical procedure, the Co-OH-CO_3/NF was used as the pre-electrode. The preparation process of the electrodeposition solution was as follows: deionized water was saturated with N_2 to remove the dissolved oxygen. $Ni(NO)_3 \cdot 6H_2O$ (0.037 g), $(NH_4)_2C_2O_4$ (0.089 g), H_3BO_3 (1.550 g), and $FeCl_2 \cdot 4H_2O$ (0.075 g) were added into 250 mL deionized water and stirred for 5 min. The electrodeposition process proceeded in a three-electrode system, and the temperature was controlled at 30 ℃.

A saturated calomel electrode was used as the reference electrode, a graphite plate electrode was used as the counter electrode. The Co-OH-CO_3/NF (2 cm × 2.5 cm) was used as the working electrode. The synthesis of the electrode had an electrodeposition time of 600 s at the current density of 5 mA cm^{-2}. The obtained self-supporting electrode was denoted as NiFe LDHs@Co-OH-CO_3/NF. To optimize the ordered nanorod electrode, different electrodeposition current densities of 0.2 mA·cm^{-2}, 2 mA·cm^{-2}, and 10 mA·cm^{-2} were also studied. The obtained self-supporting electrodes were denoted as NiFe LDHs@Co-OH-CO_3/NF-0.2, NiFe LDHs@Co-OH-CO_3/NF-2, and NiFe LDHs@Co-OH-CO_3/NF-10, respectively.

2.2.3 Preparation of NiFe LDHs/NF

For comparison, the NiFe LDHs nanosheets were prepared on the NF substrates by electrodeposition method. Typically, deionized water needed for preparing the solution was bubbled with N_2 for 30 min to remove the dissolved oxygen. $Ni(NO)_3·6H_2O$ (0.037 g), $(NH_4)_2C_2O_4$ (0.089 g), H_3BO_3 (1.550 g), and $FeCl_2·4H_2O$ (0.075 g) were added into 250 mL deionized water and stirred for 5 min to obtain the electrodeposition solution. The electrodeposition process was carried out in a three-electrode system at 30 ℃. The graphite plate was used as the counter electrode, the saturated calomel electrode was used as the reference electrode, and the previous NF (2 cm × 2.5 cm) was used as the working electrode. The electrode was obtained by an electrodeposition current density of 5 mA·cm^{-2} and an electrodeposition time of 600 s. Finally, the obtained self-supporting NiFe LDHs nanosheets electrode was denoted as NiFe LDHs/NF.

2.2.4 Preparation of the AEMWE Single-Cell

In a typical procedure, the AEMWE single-cell consisted of an anode (NiFe LDHs@Co-OH-CO_3/NF, 2 cm × 2 cm), a cathode (0.4 mg·cm^{-2} of 70wt.% Pt/C) coated on an anion exchange membrane (A201, Tokuyama), 2 cm × 2 cm, and a gas diffusion layer (carbon paper, Toray)[33, 34]. Then, the anode, the cathode coated on the alkaline anion exchange membrane, and the carbon paper were hot-pressed at 60 ℃ and 0.1 MPa for 2 min to obtain the membrane electrode assembly (MEA, NiFe LDHs@Co-OH-CO_3/NF||70% Pt/C)[35, 36]. Then, the MEA was encapsulated with the anode end plate and the cathode end plate. Finally, the AEMWE was assembled (Figure S1).

2.3 Material Characterizations

The morphologies and microstructures of the catalysts were characterized by scanning electron microscope (SEM, JSM-7800F) and transmission electron microscope (TEM, JEM-2100F), respectively. X-ray photoelectron spectra (XPS) were recordedon the ESCALAB 250Xi (Thermo escalab), using Al K_α monochrome X-ray diffraction (XRD) measurements were performed on D8-ADNANCE X-ray diffraction spectrometer (GRE, Bruker) using Cu K_α resource.

2.4 Electrochemical Measurements

All electrochemical measurements were carried out on Gamry Interface 1000e electrochemical workstation in 1 mol·L^{-1} KOH (pH = 14, O_2 saturated) at room temperature. In a three-electrode system, the voltage has been converted to reversible hydrogen electrode (RHE) based on[37-39]:

$$E_{RHE} = E_{Hg/Hg0} + 0.059pH + 0.098 \quad (1)$$

The overpotential is calculated according to[40]

$$\eta = E_{RHE} - 1.23\ V \quad (2)$$

The electrode was activated by cyclic voltammetry (CV) for 30 cycles. Linear sweep voltammetry (LSV) was used to evaluate the activity of the catalysts between 0 ~ 1 V (V vs. Hg/HgO) at a scan rate of 5 mV·s^{-1}. Electrochemical impedance spectroscopy (EIS) was employed to test the catalysts at 0.6 V (V vs. Hg/HgO), with an amplitude of 5 mV in a frequency range from 0.1 Hz to 100 kHz. The multi-step chronopotentiometric experiment was carried out sequentially at 50, 100, 150, 200, 250, and 300 mA·cm^{-2} for 300 s. The single chronopotentiometric test was carried out at a current density of 20 mA·cm^{-2} for 30 h. The electrochemically active surface area (ECSA) was measured by the CV method at different scan rates in the non-Faradaic region[28, 41].

The NiFe LDHs@Co-OH-CO_3/NF was further assembled into an AEMWE single-cell (2 cm × 2 cm) for performance testing. Current-voltage (*I*-*V*) curves were measured at 70 ℃. 1 mol·L^{-1} KOH was supplied into

the anode at a flow rate of 5 mL·min^{-1}. The stability test was conducted at a current density of 0.5 A·cm^{-2} for 100 h. The AEMWE single-cell charge transfer resistance and ohmic resistance were analyzed by measuring EIS at 1.7 V[33]. The amplitude was 10 mV and the frequency range was from 100 mHz to 10 kHz.

3 Results and Discussion

3.1 Structure and Characterization

Figure 2 shows the SEM images of NF and Co-OH-CO_3/NF. The porous morphology was observed from the NF substrate (Figure 2a), while the Co-OH-CO_3 nanowires arrays were uniformly distributed on the NF substrate (Figure 2b-d). Most of the nanowires showed a length of about 3 μm.

SEM images of NiFe LDHs/NF at different magnifications are given in Figure 3a-d. It can be seen that the NiFe LDHs nanosheets grew vertically and crossed each other in the NF substrate to form a porous array, which exposes a large number of active sites.

The uniform and ordered self-supporting NiFe LDHs@Co-OH-CO_3/NF nanorod array electrodes were obtained by optimizing the current density in electrodeposition (Figure S2). Figure 4a-d presents the SEM images of the NiFe LDHs@Co-OH-CO_3/NF electrode at different magnifications. The surface of the Co-OH-CO_3/NF was uniformly coated with the interlaced NiFe LDHs nanosheets to form the new ordered nanorod array structure, the nanorod had a diameter of about 300 nm in Figure 4b-d. The elemental mapping images shown in Figure 4e-i implied that the Co, Ni, Fe, and O elements were highly dispersed. The results showed that the self-supporting NiFe LDHs@Co-OH-CO_3/NF ordered nanorod array electrode has been successfully prepared.

TEM image of the NiFe LDHs@Co-OH-CO_3 given in Figure 5a shows the nanorod surface covered with folds and flakes. The diameter of the nanorod was about 300 nm. Figure 5b-e shows the element mapping images, while the contents of Co, Ni, Fe, and O elements, and the EDS spectra are given in Table S1 and Figure S3, respectively. This is consistent with the SEM results as shown in Figure 4. These results further show that the self-supporting NiFe LDHs@Co-OH-CO_3/NF electrodes have been successfully synthesized. The layered structure leads to the exposure of more active sites[35, 37, 42], which is conducive to

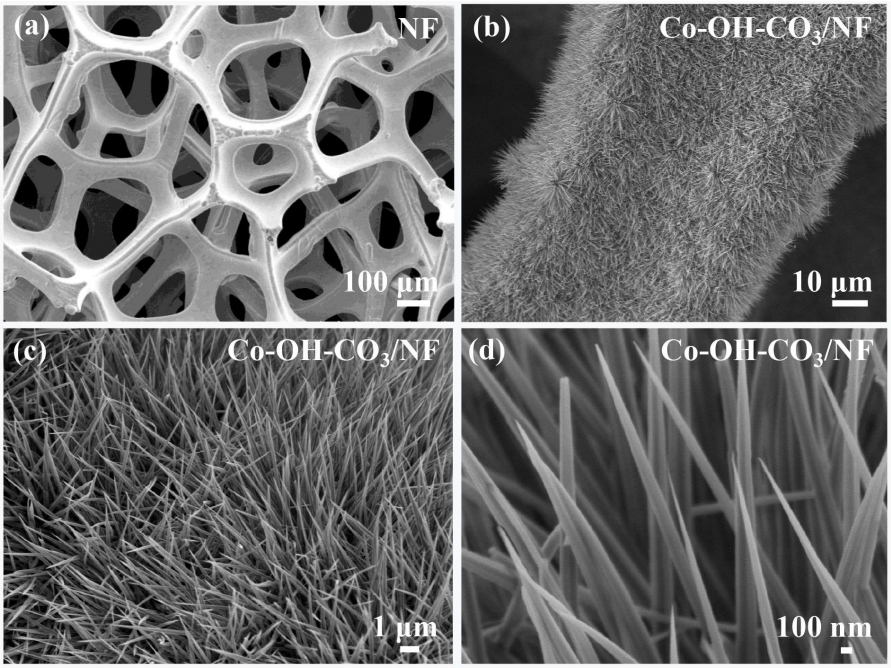

Figure 2 SEM images of NF (a) and Co-OH-CO_3/NF (b, c, and d).

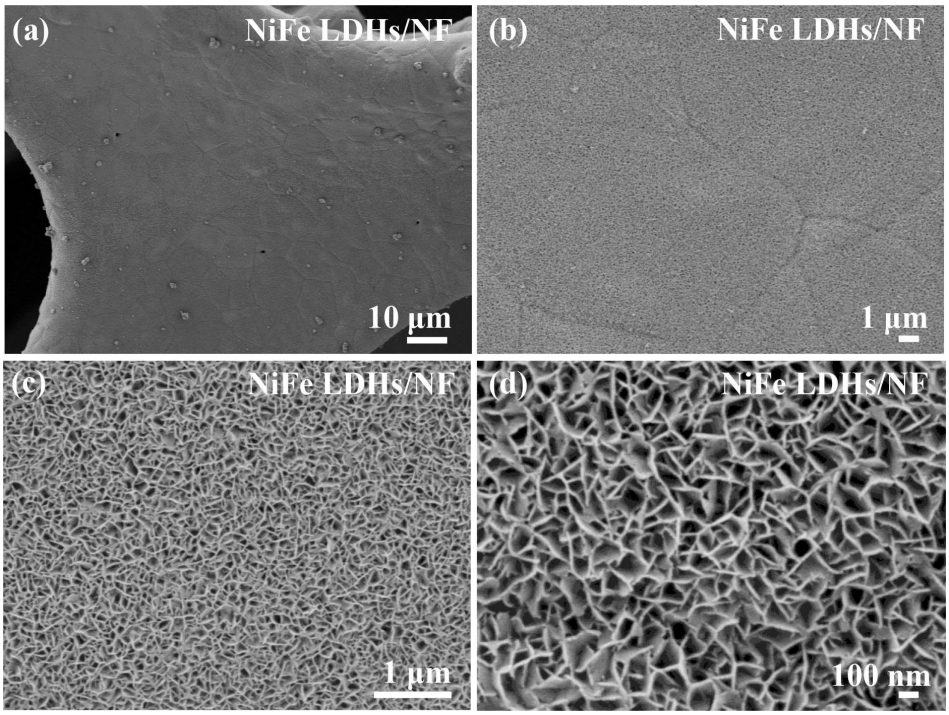

Figure 3 SEM images of the NiFe LDHs/NF (a, b, c, and d).

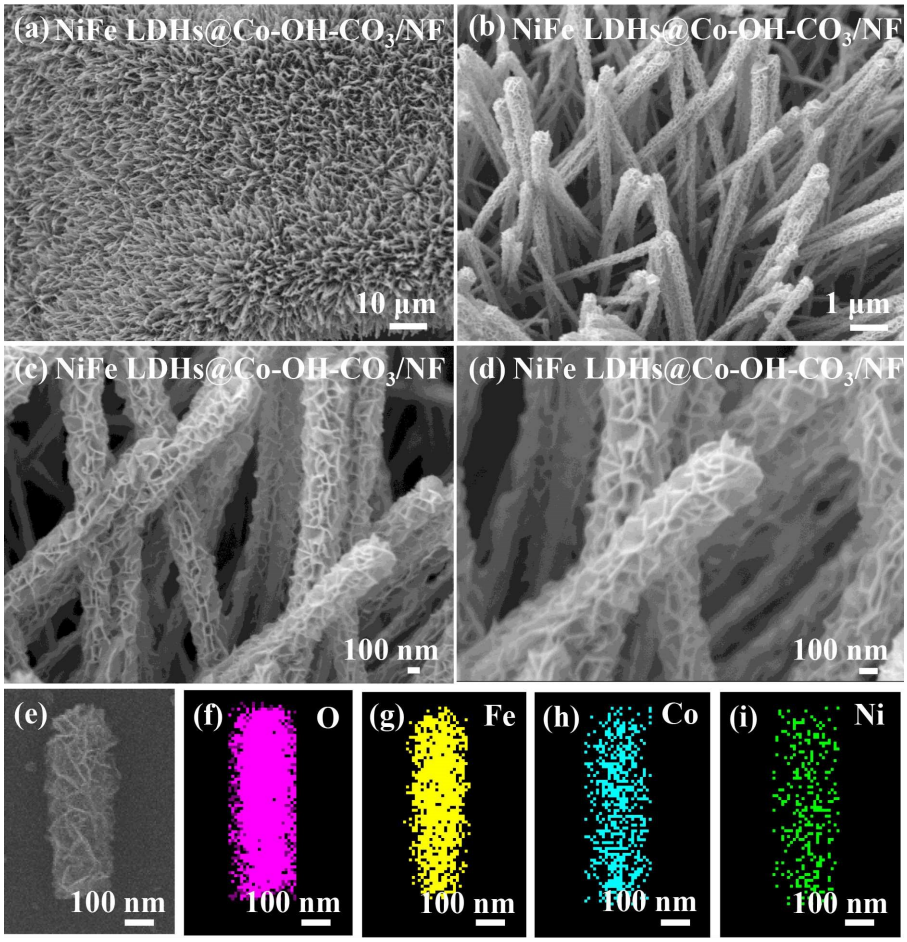

Figure 4 SEM images of the NiFe LDHs@Co-OH-CO_3/NF (a, b, c, and d) and EDS mapping images (e, f, g, h, and i). (color on line)

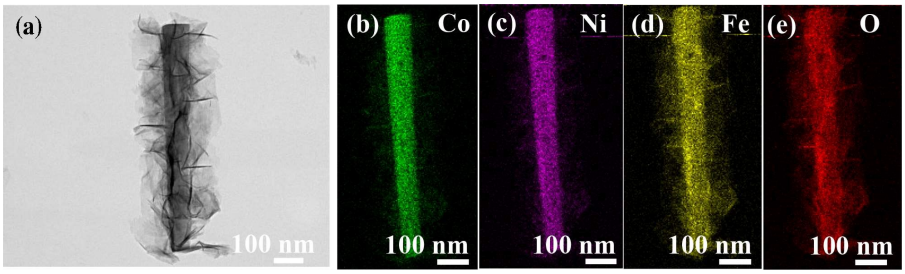

Figure 5 TEM images of the NiFe LDHs@Co-OH-CO (a), and the EDS of mapping images (b, c, d, and e). (color on line)

rapid electron transfer and gas diffusion[35].

The phase information of the prepared NF, Co-OH-CO_3/NF, NiFe LDHs/NF, and NiFe LDHs@Co-OH-CO_3/NF electrodes is provided in Figure 6a. As evident in XRD patterns shown in Figure 6a, Three stronger diffraction peaks at 44.3°, 51.7°, and 76.2° corresponded to the (111), (200), and (220) crystal planes of metal Ni (PDF#87-0712) fragment from NF[43,44]. The diffraction peaks at 17.2°, 28.7°, 30.4°, 33.8°, 35.4°, 39.5°, and 47.3° corresponded to the (020), (121), (300), (221), (040), (231), and (340) crystal planes of the Co-OH-CO_3/NF (PDF#48-0083)[31]. The peaks at 11.4°, 23.1°, 34.3°, 38.8°, 46.3°, 59.8°, and 61.2° corresponded to the (003), (006), (012), (015), (018), (110), and (113) crystal planes of NiFe LDHs (PDF#40-0215)[31, 35, 44]. This further confirms that the NiFe LDHs nanosheets were coated onto Co-OH-CO_3 nanowires array self-supporting NiFe LDHs@Co-OH-CO_3/NF electrode.

The chemical properties of the element and valence state were characterized by X-ray photoelectron spectroscopy (XPS)[45,46]. Figure 6b shows the XPS survey scan of the self-supporting NiFe LDHs@Co-OH-CO_3/NF electrode, which can further verify the existences of Fe, Ni, Co, and O elements. The XPS spectra for the fitted results of Co 2p, Ni 2p, Fe 2p, and O1s are given in Figure 6c-6e, respectively. Figure 6c shows the Co 2p spectrum has two characteristic peaks at 780.7 eV and 796.7 eV, which are ascribed to the Co $2p_{3/2}$ and Co $2p_{1/2}$, respectively, with two satellite peaks (defined as Sat.), corresponding to Co^{2+} in the Co-OH-CO_3/NF electrode[47,48]. Figure 6d shows the Ni 2p spectrum having two characteristic peaks at 855.5 eV and 873.3 eV, which are ascribed to the Ni $2p_{3/2}$ and Ni $2p_{1/2}$, respectively, with two Sat. peaks, indicating that Ni^{2+} has the typical characteristic peak of $Ni(OH)_2$[27, 31]. Figure 6e shows the Fe 2p spectrum with two characteristic peaks at 711.2 eV and 725.3 eV, ascribed to the Fe $2p_{3/2}$ and Fe $2p_{1/2}$, respectively, and two Sat. peaks,. These peaks are typical characteristic peaks of Fe^{3+}, which indicates that iron ions exist in the form of Fe^{3+} in the compound[27]. As shown in Figure 6f, there are three types of oxygen species, namely, metal-oxygen (529.2 eV), the -OH functional group in oxyhydroxide (530.8 eV), and the C=O functional group (532.5 eV)[28,49]. Previous studies have shown that the existences of transition metals Fe, Co, and Ni species are beneficial to improving OER performances[35].

3.2 OER Performance in Alkaline Media

The OER performance of the self-supporting NiFe LDHs@Co-OH-CO_3/NF electrode was tested in a three-electrode system and 1 mol·L^{-1} KOH at 25 °C. For comparison, the OER performance of the NF electrode, Co-OH-CO_3/NF electrode, and NiFe LDHs/NF electrode were also tested as shown in Figure 7a-b. The LSV (without iR-correction) curves showed that the NF electrode performance was poor, and the overpotential of 330 mV at the current density of 20 mA·cm^{-2} is given in Figure 7a. When the Co-OH-CO_3 nanowire array was vertically coated onto the NF, the Co-OH-CO_3/NF electrode performance was improved (295 mV at 20 mA·cm^{-2}). The NiFe LDHs nanosheets were vertically coated onto the NF by electrodeposition (NiFe LDHs/NF) with the overpotential of 255 mV at the current density of 20 mA·cm^{-2}. The performance of the NiFe LDHs/NF electrode (255 mV at 20 mA·cm^{-2} and 350 mV at 100 mA·cm^{-2}) was better

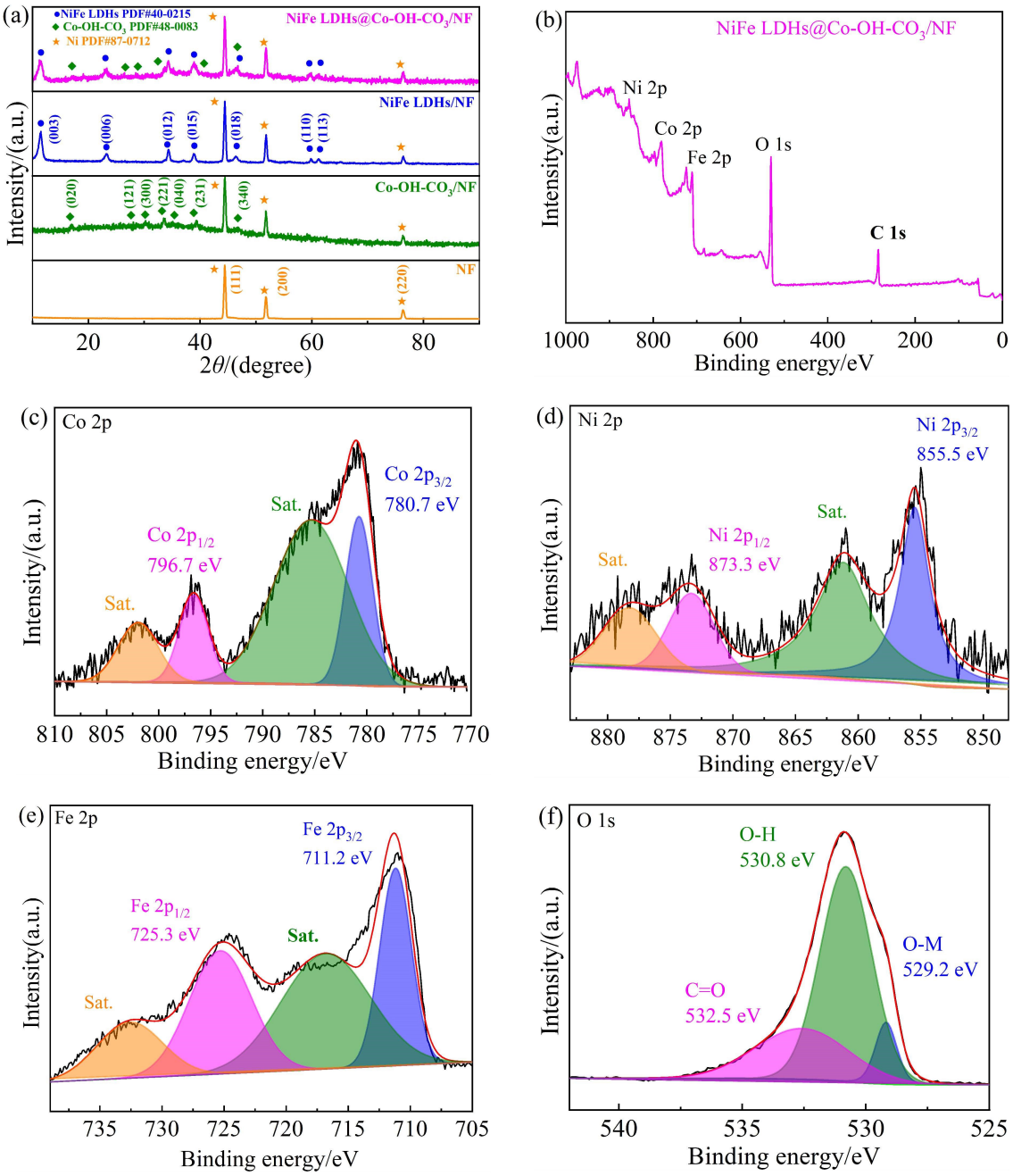

Figure 6 (a) XRD patterns of NF, Co-OH-CO_3/NF, NiFe LDHs/NF, and NiFe LDHs@Co-OH-CO_3/NF electrodes; XPS survey spectra (b) and XPS fine spectra (c-f) of NiFe LDHs@Co-OH-CO_3/NF electrode. (c) Co 2p; (d) Ni 2p; (e) Fe 2p; (f) O 1s. (color on line)

than those of the Co-OH-CO_3/NF electrode (295 mV at 20 mA·cm^{-2} and 400 mV at 100 mA·cm^{-2}) and the NF electrode (330 mV at 20 mA·cm^{-2} and 435 mV at 100 mA·cm^{-2}) in Figure 7b. The result reveals that the nanosheets in the NiFe LDHs/NF electrode are crosslinked to produce a large number of voids, which makes the NiFe LDHs/NF electrode easy to access electrolyte and has better OER performance[35]. Among them, the self-supporting NiFe LDHs@Co-OH-CO_3/NF electrode showed the best performance with overpotentials of only 215 mV and 310 mV at the current densities of 20 and 100 mA·cm^{-2}, respectively. There is an obvious oxidation peak in the LSV curve of the Co-OH-CO_3/NF electrode, which is the oxidation peaks of Ni and Co[50, 51], while in the LSV curve of the NiFe LDHs@Co-OH-CO_3/NF electrode,

the oxidation peak shifts to the left[51, 52] and the peak intensity decreases, indicating that Fe has been successfully doped, and the NiFe LDHs have uniformly distributed and coated onto the Co-OH-CO_3/NF electrode. The different electrodeposition current densities in the preparations of NiFe LDHs@Co-OH-CO_3/NF-0.2 electrode, NiFe LDHs@Co-OH-CO_3/NF-2 electrode, and NiFe LDHs@Co-OH-CO_3/NF-10 electrode at 20 mA·cm^{-2}, the overpotential reaches 255 mV, 250 mV, and 245 mV, respectively (in Figure S4). The NiFe LDHs@Co-OH-CO_3/NF electrode has previously shown the excellent OER performance (see

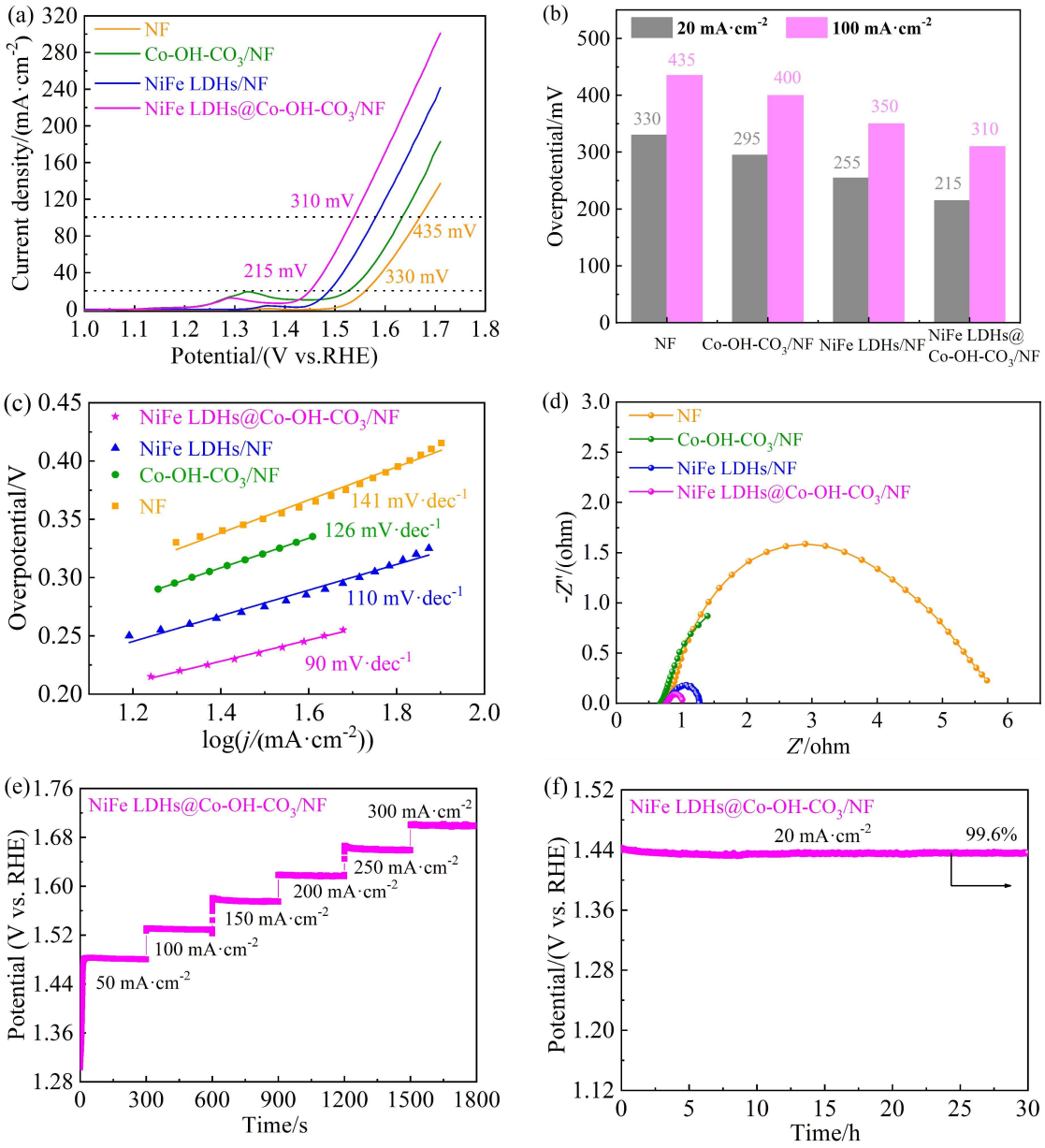

Figure 7 The OER performances tested in a three-electrode system and 1 mol·L^{-1} KOH. (a) LSV curves of NF electrode, Co-OH-CO_3/NF electrode, Co-OH-CO_3/NF electrode, and NiFe LDHs@Co-OH-CO_3/NF electrode with a scan rate of 5 mV·s^{-1} at room temperature; (b) the comparison of overpotential at 20 and 100 mA·cm^{-2} for NiFe LDHs@Co-OH-CO_3/NF electrode and other electrodes; (c) the corresponding Tafel plots; (d) Nuquist plots of NF electrode, Co-OH-CO_3/NF electrode, NiFe LDHs/NF electrode, and NiFe LDHs@Co-OH-CO_3/NF electrode; (e) multi-step chronopotentiometric curves of NiFe LDHs@Co-OH-CO_3/NF electrode by varying current density from 50 to 300 mA·cm^{-2} with an increment of 50 mA·cm^{-2} for 300 s; (f) chronopotentiometric curves of NiFe LDHs@Co-OH-CO_3/NF electrode at 20 mA·cm^{-2} for 30 h. (color on line)

table 1)[28, 42, 44, 53-58]. The result is attributed to the self-supporting NiFe LDHs@Co-OH-CO_3/NF electrode with a unique ordered nanorod array structure, which exposes more active sites and accelerates electron transfer and gas diffusion, so it shows good OER performance[35].

The Tafel slope was obtained by linear fitting to analyze the kinetics of the OER reaction process. As presented in Figure 7c, the Tafel slopes of the NF electrode, Co-OH-CO_3/NF electrode, NiFe LDHs/NF electrode, and NiFe LDHs@Co-OH-CO_3/NF electrode were 141, 126, 110, and 90 mV·dec^{-1}, respectively. Particularly, the NiFe LDHs@Co-OH-CO_3/NF electrode had the smallst slope, which further indicates that the NiFe LDHs@Co-OH-CO_3/NF electrode achieves a significantly fast OER kinetics[59].

EIS was used to test the charge transfer resistance (R_{ct}), which is the diameter of the semicircle in the impedance diagram, and reflects the charge transfer efficiency of the OER electrode. The Nyquist plots of the NF electrode, Co-OH-CO_3/NF electrode, NiFe LDHs/NF electrode, and NiFe LDHs@Co-OH-CO_3/NF electrode are given in Figure 7d. It can be seen that the R_{ct} decreasing order of the four OER electrodes were NF > Co-OH-CO_3/NF > NiFe LDHs/NF > NiFe LDHs@Co-OH-CO_3/NF. The R_{ct} value of the Co-OH-CO_3@NiFe LDHs/NF electrode was the smallest (about 0.3 Ω), indicating a better charge transferability in an alkaline OER.

Stability is an important index to evaluate the performance of catalysts[60]. Firstly, the potential-time curves of NiFe LDHs@Co-OH-CO_3/NF electrode were tested by chronopotentiometry (Figure 7e), and the current density was increased every 300 s from 50 mA·cm^{-2} to 300 mA·cm^{-2}. It can be seen that the potential could be stable in a certain range under different current densities, indicating that the NiFe LDHs@Co-OH-CO_3/NF electrode has good stability

Table 1 Summary of various non-noble metal catalysts for OER in alkaline solutions (25 °C).

Electrocatalyst	Substrate	η for OER at corresponding j (mV@mA cm^{-2})	Tafel slope (mV·dec^{-1})	Stability test	Reference
Fe: Ni/Ni_2P IO	nickel foam	285@20 (iR-compensated)	48	20 mA·cm^{-2} for 100 h	[53]
Ni-Fe LDH DSNCS	glassy carbon electrode	246@20 (iR-compensated)	71	20 mA·cm^{-2} for 50 h	[42]
FeOOH/Co/FeOOH HNTAs-NF	nickel foam	250@20 (iR-compensated)	-	20 mA·cm^{-2} for 50 h	[54]
NiS_2/$NiSe_2$	glassy carbon electrode	290@20 (iR-compensated)	119	100 mA·cm^{-2} for 20 h	[55]
Cu@CeO_2@NFC-0.25	copper foam	231@10 (without iR compensated)	32.7	10 and 20 mA·cm^{-2} for 30 h	[56]
NiFe-OH-PO_4/NF	nickel foam	249@20 (iR compensated)	41.8	100 mA·cm^{-2} for 10h	[57]
CoP@NiFe-OH	nickel foam	220@20 (iR-compensated)	49.6	20 mA·cm^{-2} for 24 h	[28]
CoO@NiFe LDH/NF	nickel foam	225@20 (without iR-compensated)	65	20 mA·cm^{-2} for 80 h	[44]
$Ni_{0.9}Fe_{0.1}PS_3$ NSs	glassy carbon electrode	329@20 (iR-compensated)	69	30 mA·cm^{-2} for 50 h	[58]
NiFe LDHs@Co-OH-CO_3/NF	nickel foam	215@20 (without iR compensated)	90	20 mA·cm^{-2} for 30 h	this work

under different current densities[61]. In addition, the stability of the NiFe LDHs@Co-OH-CO_3/NF electrode was evaluated by measuring the chronopotentiometric curve at a current density of 20 mA·cm^{-2} for 30 h. The potential could still maintain 99.6% of the original one (Figure 7f). LSV curves and morphology of the NiFe LDHs@Co-OH-CO_3/NF electrode after the stability test in a three-electrode system are supplied in Figure S5 and Figure S6. The morphology of the NiFe LDHs@Co-OH-CO_3/NF electrode remained almost unchanged after the stability test.

The electrochemically surface area (ECSA) of the catalyst was measured by cyclic voltammetry (CV)

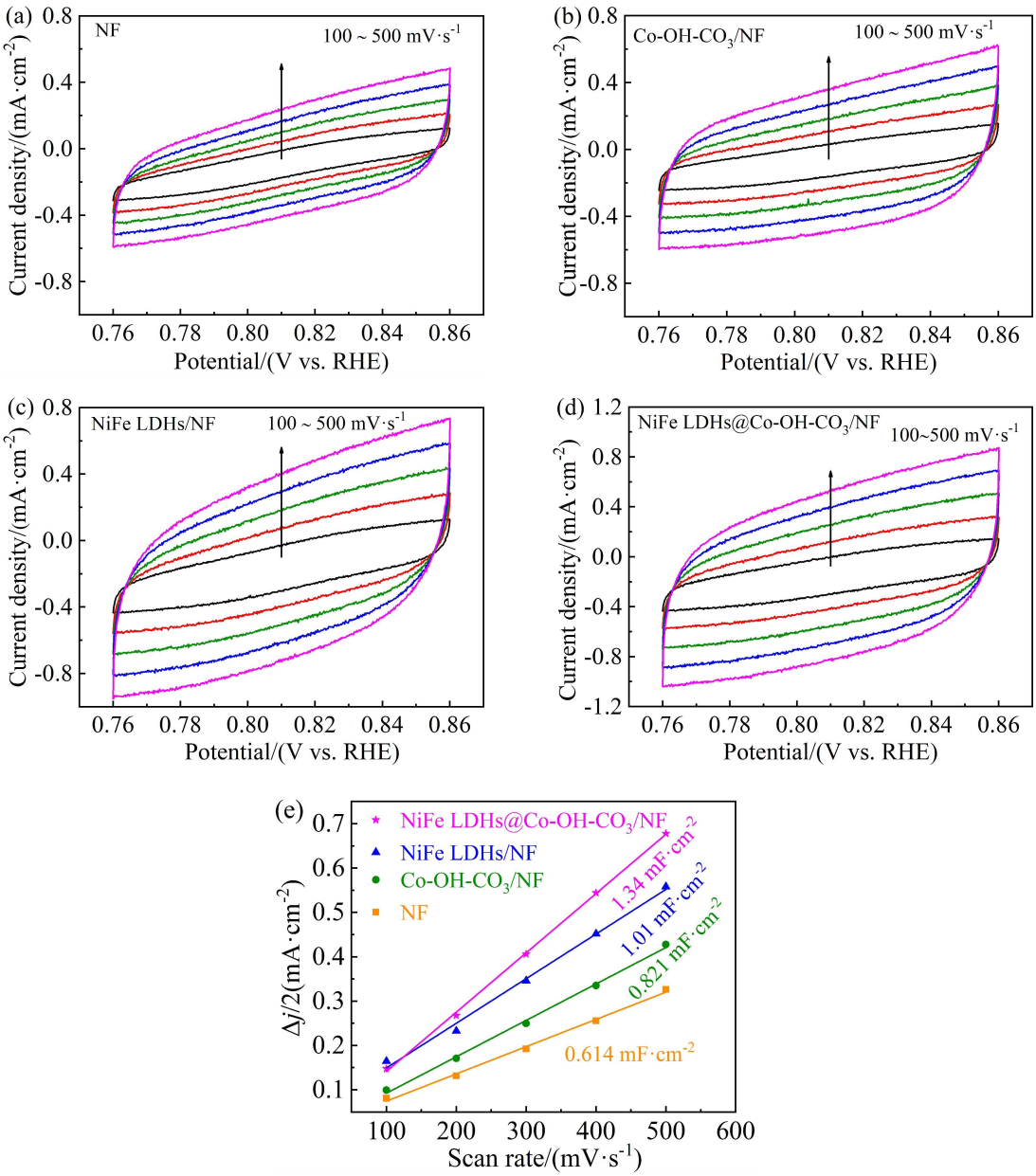

Figure 8 CV curves of NF electrode (a), Co-OH-CO_3/NF electrode (b), NiFe LDHs/NF electrode (c), and NiFe LDHs@Co-OH-CO_3/NF electrode (d) in the double-layer region at scan rates of 100, 200, 300, 400, and 500 mV·s^{-1} in 1 mol·L^{-1} KOH; (e) the C_{dl} values of NF electrode, Co-OH-CO_3/NF electrode, NiFe LDHs/NF electrode and NiFe LDHs@Co-OH-CO_3/NF electrode determined by plots of $\Delta j/2 = (j_{ab} - j_c)/2$ as a function of scan rate for with different shells. j_a represents the anode current density, j_c represents the cathode current density. (color on line)

according to the double-layer capacitance (C_{dl})[62]. The C_{dl} of the catalyst is positively correlated with ECSA. The greater ECSA of the electrode, the better the corresponding catalytic performance[41, 63, 64]. Figure 8a-d shows the CV curves of the NF electrode, Co-OH-CO_3/NF electrode, NiFe LDHs/NF electrode, and NiFe LDHs@Co-OH-CO_3/NF electrode at 0.76 ~ 0.86 V (vs. RHE) with scanning speeds of 100, 200, 300, 400, and 500 mV·s^{-1}. The ECSA of the materials can be calculated by CV curves. Figure 8e shows that the C_{dl} values of NF electrode, Co-OH-CO_3/NF electrode, NiFe LDHs/NF electrode, and NiFe LDHs@Co-OH-CO_3/NF electrode were 0.614, 0.821, 1.01, and 1.34 mF·cm^{-2}, respectively. It can be seen that the NiFe LDHs@Co-OH-CO_3/NF electrode had the largest C_{dl} of 1.34 mF·cm^{-2}, which further indicates that the NiFe LDHs@Co-OH-CO_3/NF electrode has more active sites and excellent OER performance[37]. In addition, the ECSA normalized LSV curves of the Co-OH-CO_3/NF electrode, NiFe LDHs/NF electrode, and NiFe LDHs@Co-OH-CO_3/NF electrode are presented in Figure S7 to reflect the intrinsic activity of different samples. The NiFe LDHs@Co-OH-CO_3/NF electrode exhibited the enhanced relative ECSA normalized OER activity than those of the NiFe LDHs/NF electrode and the Co-OH-CO_3/NF electrode.

3.3 Performance of NiFe LDHs@Co-OH-CO_3/NF Electrode as the Anode of the AEMWE Single-Cell

To test the potential application of the NiFe LDHs@Co-OH-CO_3/NF electrode as an anode of the AEMWE in 1 mol·L^{-1} KOH at 70 °C, the cell was assembled as shown in Figure 9a. Figure 9b shows the *I-V* curves (without iR-correction) of NiFe LDHs@Co-OH-CO_3/NF||70% Pt/C. When the current densities were 0.5 and 1 A·cm^{-2}, the cell voltages reached

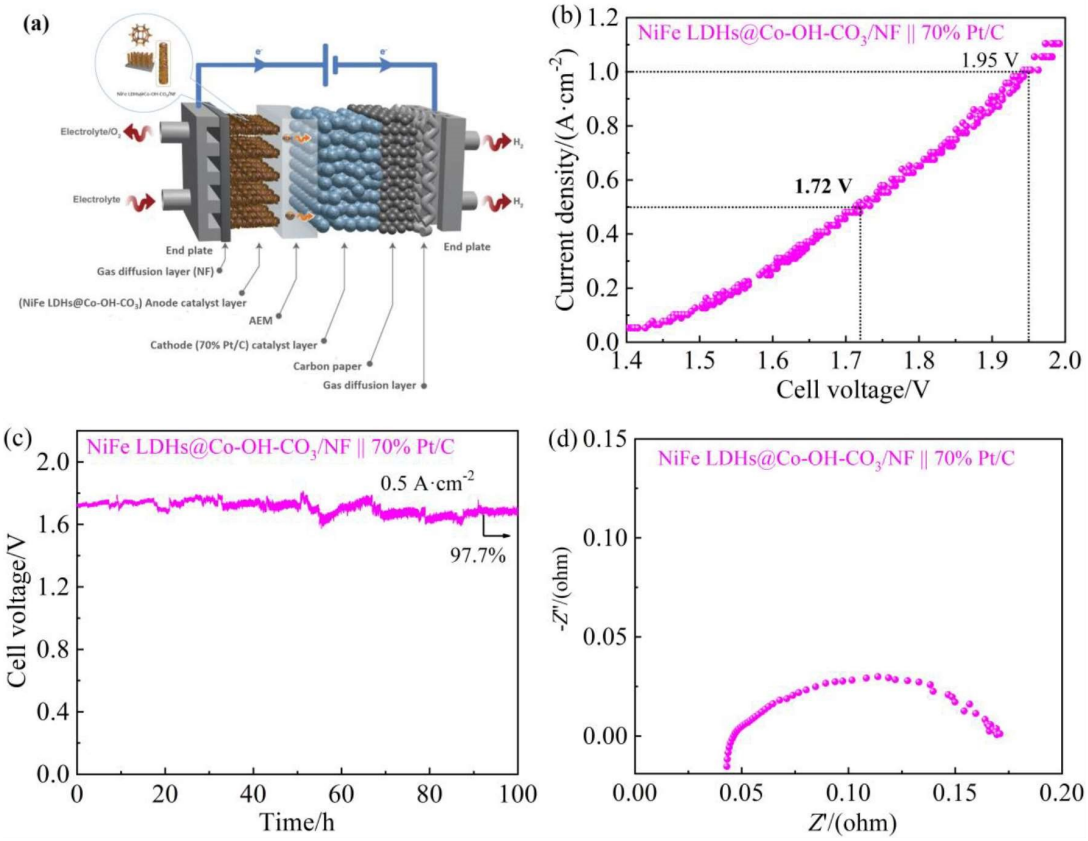

Figure 9 (a) Schematic illustration of AEMWE, (b) Current-voltage curves of the NiFe LDHs@Co-OH-CO_3/NF electrode as the anode for AEMWE single-cell at 70 °C, (c) Cell voltage-time curve from the stability test at 0.5 A·cm^{-2}, (d) Nyquist plot at 1.7 V. (color on line)

Table 2 Comparison of AEMWE performance 1 mol·L^{-1} KOH

(anode‖cathode)	Cell voltage V@ A·cm^{-2}	Cell temperature (℃)	Stability test (hours @ A·cm^{-2})	Reference
NiFeCo LDH‖NiFeCo phosphide	1.75@0.5	50	40 @ 0.5	[34]
FeOOH/NiFe LDHs@CCH NAs-NF‖70 wt% Pt/C (0.4 mg·cm^{-2})	1.768@0.5	70	100 @ 0.5	[31]
$Co(OH)_x$/Ag/$Co(OH)_2$‖40 wt% Pt/C (not mention)	1.8@0.6	50	24 @ 0.6	[33]
$VCoCO_x$@NF ‖ $VCoCO_x$@NF	2.01@0.2	45	12 @ 0.25	[36]
CE-CCO‖70 wt% Pt/C (1 mg·cm^{-2})	1.8@1.39	45	64 @ 0.5	[65]
NiFe LDHs@Co-OH-CO_3/NF‖70 wt% Pt/C(0.4 mg·cm^{-2})	1.72@0.5	70	100 @ 0.5	This work
	1.95@1	70	–	This work

1.72 and 1.95 V, respectively. According to the low calorific value of hydrogen, the electrolytic efficiencies were 86.0% and 75.9%, respectively. In addition, the prepared AEMWE single-cell required a lower cell voltage than those previously reported for non-noble metals based on AEMWEs under the similar operating conditions (Table 2)[31, 33, 34, 36, 65].

The stability of AEMWE single-cell was tested at a constant current density of 0.5 A·cm^{-2} for 100 h. The cell voltage remained at 97.7% of the original voltage (Figure 9c). The ohmic resistance and charge-transfer resistance were evaluated by the measurement of EIS at 1.7 V (about 0.5 A·cm^{-2})[33]. As shown in Figure 9d, the R_{ct} of the AEMWE single-cell was small, which means that the NiFe LDHs@Co-OH-CO_3/NF electrode has efficient charge transfer capability [35]. These results indicate that the NiFe LDHs@Co-OH-CO_3/NF electrode is highly effective as a non-noble metal-based OER electrode in an AEMWE single-cell.

4 Conclusions

In summary, the 3D layered self-supporting NiFe LDHs@Co-OH-CO_3/NF nanorod array electrode has been successfully prepared. The unique morphologic structure of the NiFe LDHs@Co-OH-CO_3/NF electrode revealed the following characteristics: (1) The inner layer of Co-OH-CO_3 can effectively prevent the agglomeration of NiFe LDHs nanosheets, which is conducive to electron transfer, and provides a large number of edge and interface sites for water electrolyzer. (2) The outer layer of NiFe LDHs nanosheets crosses each other to form rich and regular pores, which not only can significantly increase the catalytic active sites, but also reduce the ion diffusion distance and transmission resistance. (3) The strong interaction can enhance the conductivity of the NiFe LDHs@Co-OH-CO_3/NF electrode between NiFe LDHs@Co-OH-CO_3 and NF substrate. As a result, the excellent performances were achieved both in a three-electrode system and in an AEMWE single-cell as the anode. The NiFe LDHs@Co-OH-CO_3/NF electrode exhibited the excellent OER activity with a low overpotential 215 mV at the current density of 20 mA·cm^{-2} and good stability for 30 h in 1 mol·L^{-1} KOH. In addition, the NiFe LDHs@Co-OH-CO_3/NF electrode as the anode of the AEMWE also showed the good performance in 1 mol·L^{-1} KOH at 70 ℃. The cell voltage was 1.72 V at the current density of 0.5 A·cm^{-2} with the excellent stability for 100 h. This study provides useful guidance for the design of the anode for AEMWEs.

Acknowledgments:

This work was supported by the Key Program of the National Natural Science Foundation of China (No. 22090032, 22090030), the Joint Fund of the Yulin University and the Dalian National Laboratory for Clean Energy (Grant. YLU-DNL Fund 2021001). In addition, we sincerely appreciate the support from the Dalian Key Laboratory of Electrolysis for Hydro-

gen Production.

References:

[1] Zhang Z, Li X P, Zhong C, Zhao N Q, Deng Y D, Han X P, Hu W B. Spontaneous synthesis of silver-nanoparticle-decorated transition metal hydroxides for enhanced oxygen evolution reaction[J]. Angew. Chem. Int. Ed., 2020, 59(18): 7245-7250.

[2] Xie X Y, Cao C S, Wei W B, Zhou S H, Wu X T, Zhu Q L. Ligand-assisted capping growth of self-supporting ultrathin FeNi-LDH nanosheet arrays with atomically dispersed chromium atoms for efficient electrocatalytic water oxidation[J]. Nanoscale, 2020, 12(10): 5817-5823.

[3] Lv L, Yang Z X, Chen K, Wang C D, Xiong Y J. 2D layered double hydroxides for oxygen evolution reaction: from fundamental design to application[J]. Adv. Energy Mater., 2019, 9(17): 1803358.

[4] You B, Zhang Y D, Jiao Y, Davey K, Qiao S Z. Negative charging of transition-metal phosphides via strong electronic coupling for destabilization of alkaline water[J]. Angew. Chem. Int. Ed., 2019, 58(34): 11796-11800.

[5] Qi J, Lin Y P, Chen D D, Zhou T H, Zhang W, Cao R. Autologous cobalt phosphates with modulated coordination sites for electrocatalytic water oxidation[J]. Angew. Chem. Int. Ed., 2020, 59(23): 8917-8921.

[6] Yao R Q, Shi H, Wan W B, Wen Z, Lang X Y, Jiang Q. Flexible Co-Mo-N/Au electrodes with a hierarchical nanoporous architecture as highly efficient electrocatalysts for oxygen evolution reaction[J]. Adv. Mater., 2020, 32(10): 1907214.

[7] Javaid S, Xu X M, Chen W, Chen J Y, Hsu H Y, Wang S, Yang X Y, Li Y G, Shao Z P, Jones F, Jia G H. Ni^{2+}/Co^{2+} doped Au-Fe_7S_8 nanoplatelets with exceptionally high oxygen evolution reaction activity[J]. Nano Energy, 2021, 89: 106463.

[8] Jiang G, Yu H M, Li Y H, Yao D W, Chi J, Sun S C, Shao Z G. Low-loading and highly stable membrane electrode based on an Ir@WO_xNR ordered array for PEM water electrolysis[J]. ACS Appl. Mater. Interfaces, 2021, 13(13): 15073-15082.

[9] Moriau L, Bele M, Marinko Ž, Ruiz-Zepeda F, Podboršek G K, Šala M, Šurca A K, Kovač J, Arcon I, Jovanovic P, Hodnik N, Suhadolnik L. Effect of the morphology of the high-surface-area support on the performance of the oxygen-evolution reaction for iridium nanoparticles[J]. ACS Catal., 2021, 11(2): 670-681.

[10] Yao Q, Huang B L, Xu Y, Li L G, Shao Q, Huang X Q. A chemical etching strategy to improve and stabilize RuO_2-basd nano assemblies for acidic oxygen evolution [J]. Nano Energy, 2021, 84: 105909.

[11] Han X P, Ling X F, Yu D S, Xie D Y, Li L L, Peng S J, Zhong C, Zhao N Q, Deng Y D, Hu W B. Atomically dispersed binary Co-Ni sites in nitrogen-doped hollow carbon nanocubes for reversible oxygen reduction and evolution[J]. Adv. Mater., 2019, 31(49): 1905622.

[12] Sun S N, Sun Y M, Zhou Y, Xi S B, Ren X, Huang B C, Liao H B, Wang L Y P, Du Y H, Xu Z C. Shifting oxygen charge towards octahedral metal: a way to promote water oxidation on cobalt spinel oxides[J]. Angew. Chem. Int. Ed., 2019, 58(18): 6042-6047.

[13] Chen J S, Li H, Chen S M, Fei J Y, Liu C, Yu Z X, Shin K, Liu Z W, Song L, Henkelman G, Wei L, Chen Y. Co-Fe-Cr (oxy)hydroxides as efficient oxygen evolution reaction catalysts[J]. Adv. Energy Mater., 2021, 11(11): 2003412.

[14] Guo X L, Zheng X Q, Hu X L, Zhao Q N, Li L, Yu P, Jing C, Zhang Y X, Huang G S, Jiang B, Xu C H, Pan F S. Electrostatic adsorbing graphene quantum dot into nickel-based layered double hydroxides: Electron absorption/donor effects enhanced oxygen electrocatalytic activity[J]. Nano Energy, 2021, 84: 105932.

[15] Wang Y, Yan L T, Dastafkan K, Zhao C, Zhao X B, Xue Y Y, Huo J M, Li S N, Zhai Q G. Lattice matching growth of conductive hierarchical porous MOF/LDH heteronanotube arrays for highly efficient water oxidation [J]. Adv. Mater., 2021, 33(8): 2006351.

[16] Wang Y, Liu B R, Shen X J, Arandiyan H, Zhao T W, Li Y B, Garbrecht M, Su Z, Han L, Tricoli A, Zhao C. Engineering the activity and stability of MOF-nanocomposites for efficient water oxidation[J]. Adv. Energy Mater., 2021, 11(16): 2003759.

[17] Gao L K, Cui X, Wang Z W, Sewell C D., Li Z L, Liang S, Zhang M Y, Li J, Hu Y J, Lin Z Q. Operando unraveling photothermal-promoted dynamic active-sites generation in $NiFe_2O_4$ for markedly enhanced oxygen evolution [J]. PNAS, 2021, 118(7): e2023421118.

[18] Wang K, Du H F, He S, Liu L, Yang K, Sun J M, Liu Y H, Du Z Z, Xie L H, Ai W, Huang W. Kinetically controlled, scalable synthesis of γ-FeOOH nanosheet arrays on nickel foam toward efficient oxygen evolution: The key role of *in-situ*-generated γ-NiOOH[J]. Adv. Mater., 2021, 33(11): 2005587.

[19] Hao Y M, Li Y F, Wu J X, Meng L S, Wang J L, Jia C L, Liu T, Yang X J, Liu Z P, Gong M. Recognition of surface oxygen intermediates on NiFe oxyhydroxide oxygen-evolving catalysts by homogeneous oxidation reac-

tivity[J]. J. Am. Chem. Soc., 2021, 143(3): 1493-1502.

[20] Liu P, Chen B, Liang C W, Yao W T, Cui Y Z, Hu S Y, Zou P C, Zhang H, Fan H J, Yang C. Tip-enhanced electric field: A new mechanism promoting mass transfer in oxygen evolution reactions[J]. Adv. Mater., 2021, 33(9): 2007377.

[21] Tran D T, Le H T, Hoa V H, Kim N H, Lee J H. Dual-coupling ultrasmall iron-Ni_2P into P-doped porous carbon sheets assembled Cu_xS nanobrush arrays for overall water splitting[J]. Nano Energy, 2021, 84: 105861.

[22] Han L, Dong S J, Wang E K. Transition-metal (Co, Ni, and Fe)-based electrocatalysts for the water oxidation reaction[J]. Adv. Mater., 2016, 28(42): 9266-9291.

[23] Kargar A, Yavuz S, Kim T K, Liu C-H, Kuru C, Rustomji C S, Jin S, Bandaru P R. Solution-processed $CoFe_2O_4$ nanoparticles on 3D carbon fiber papers for durable oxygen evolution reaction[J]. ACS Appl. Mater. Interfaces, 2015, 7(32): 17851-17856.

[24] Shah J H, Xie Q X, Kuang Z C, Ge R L, Zhou W H, Liu D R, Rykov A I, Li X N, Luo J S, Wang J H. *In-situ*/operando ^{57}Fe mössbauer spectroscopic technique and its applications in NiFe-based electrocatalysts for oxygen evolution reaction[J]. J. Electrochem., 2022, 28(3): 51-81.

[25] Zhao J, Zhang J J, Li Z Y, Bu X H. Recent progress on NiFe-based electrocatalysts for the oxygen evolution reaction[J]. Small, 2020, 16(51): 2003916.

[26] Dionigi F, Strasser P. NiFe-based (oxy)hydroxide catalysts for oxygen evolution reaction in non-acidic electrolytes[J]. Adv. Energy Mater., 2016, 6(23): 1600621.

[27] Chi J, Yu H M, Qin B W, Fu L, Jia J, Yi B L, Shao Z G. Vertically aligned FeOOH/NiFe layered double hydroxides electrode for highly efficient oxygen evolution reaction[J]. ACS Appl. Mater. Interfaces, 2017, 9(1): 464-471.

[28] Li Y, Guo S W, Jin T, Wang Y L, Cheng F Y, Jiao L F. Promoted synergy in core-branch CoP@NiFe-OH nanohybrids for efficient electrochemical-/photovoltage-driven overall water splitting[J]. Nano Energy, 2019, 63: 103821.

[29] Zhao Y F, Zhang X, Jia X D, Waterhouse G I N., Shi R, Zhang X R, Zhan F, Tao Y, Wu L Z, Tung C H, O'Hare D, Zhang T R. Sub-3 nm ultrafine monolayer layered double hydroxide nanosheets for electrochemical water oxidation[J]. Adv. Energy Mater., 2018, 8(18): 1703585.

[30] Kuai C G, Zhang Y, Wu D Y, Sokaras D, Mu L Q, Spence S, Nordlund D, Lin F, Du X W. Fully oxidized Ni-Fe layered double hydroxide with 100% exposed active sites for catalyzing oxygen evolution reaction[J]. ACS Catal., 2019, 9(7): 6027-6032.

[31] Chi J, Yu H M, Jiang G, Jia J, Qin B W, Yi B L, Shao Z G. Construction of orderly hierarchical FeOOH/NiFe layered double hydroxides supported on cobaltous carbonate hydroxide nanowire arrays for a highly efficient oxygen evolution reaction[J]. J. Mater. Chem. A, 2018, 6(8): 3397-3401.

[32] Jeon S S, Lim J, Kang P W, Lee J W, Kang G, Lee H. Design principles of NiFe-layered double hydroxide anode catalysts for anion exchange membrane water electrolyzers[J]. ACS Appl. Mater. Interfaces, 2021, 13(31): 37179-37186.

[33] Guo W W, Kim J, Kim H, Han G H, Jang H W, Kim S Y, Ahn S H. Sandwich-like $Co(OH)_x$/Ag/$Co(OH)_2$ nanosheet composites for oxygen evolution reaction in anion exchange membrane water electrolyzer[J]. J. Alloys Compd., 2021, 889: 161674.

[34] Lee J, Jung H, Park Y S, Kwon N, Woo S, Selvam N. C S, Han G S, Jung H S, Yoo P J, Choi S M, Han J W, Lim B. Chemical transformation approach for high-performance ternary NiFeCo metal compound-based water splitting electrodes[J]. Appl. Catal., B, 2021, 294: 120246.

[35] Zhang H, Shen G Q, Liu X Y, Ning B, Shi C X, Pan L, Zhang X W, Huang Z F, Zou J J. Self-supporting NiFe LDH-MoS_x integrated electrode for highly efficient water splitting at the industrial electrolysis conditions[J]. Chin. J. Catal., 2021, 42(10): 1732-1741.

[36] Meena A, Thangavel P, Nissimagoudar A S, Singh A N, Jana A, Jeong D S, Im H, Kim K S. Bifunctional oxovanadate doped cobalt carbonate for high-efficient overall water splitting in alkaline-anion-exchange-membrane water-electrolyzer[J]. Chem. Eng. J., 2022, 430: 132623.

[37] Wang J Y, Li S M, Lin R B, Tu G M, Wang J, Li Z Q. MOF-derived hollow β-FeOOH polyhedra anchored with α-$Ni(OH)_2$ nanosheets as efficient electrocatalysts for oxygen evolution[J]. Electrochim. Acta, 2019, 301: 258-266.

[38] Zhai P L, Xia M Y, Wu Y Z, Zhang G H, Gao J F, Zhang B, Cao S Y, Zhang Y T, Li Z W, Fan Z Z, Wang C, Zhang X M, Miller J T, Sun L C, Hou J G. Engineering single-atomic ruthenium catalytic sites on defective nickel-iron layered double hydroxide for overall water splitting[J]. Nat. Commun., 2021, 12(1): 4587.

[39] Han M Y, Zhang X W, Gao H Y, Chen S Y, Cheng P, Wang P, Zhao Z Y, Dang R, Wang G. *In situ* semi-sacrificial template-assisted growth of ultrathin metal-organic framework nanosheets for electrocatalytic oxygen evolution[J]. Chem. Eng. J., 2021, 426: 131348.

[40] Dou Y H, He C T, Zhang L, Yin H J, Al-Mamun M, Ma J M, Zhao H J. Approaching the activity limit of $CoSe_2$ for oxygen evolution via Fe doping and Co vacancy[J].

Nat. Commun., 2020, 11(1): 1664.

[41] Peng L S, Yang N, Yang Y Q, Wang Q, Xie X Y, Sun-Waterhouse D, Shang L, Zhang T R, Waterhouse G I N. Atomic cation-vacancy engineering of NiFe-layered double hydroxides for improved activity and stability towards the oxygen evolution reaction[J]. Angew. Chem. Int. Ed., 2021, 60(46): 24612-24619.

[42] Zhang J T, Yu L, Chen Y, Lu X F, Gao S Y, Lou X W. Designed formation of double-shelled Ni-Fe layered-double-hydroxide nanocages for efficient oxygen evolution reaction[J]. Adv. Mater., 2020, 32(16): 1906432.

[43] Yan Z, Wang E D, Gao J X, Yang J P, Wu C C, Jiang L H, Zhu M Y, Sun G Q. An exceptionally facile synthesis of high efficient oxygen evolution electrodes for zinc-oxygen batteries[J]. ChemElectroChem, 2017, 4(9): 2190-2195.

[44] Wang Z P, Zhang J H, Yu Q Y, Yang H Y, Chen X, Yuan X, Huang K, Xiong X L. Synthesis of 3D CoO nanowires supported NiFe layered double hydroxide using an atmospheric pressure microplasma for high-performance oxygen evolution reaction[J]. Chem. Eng. J., 2021, 410: 128366.

[45] Boppella R, Tan J W, Yang W, Moon J. Homologous CoP/NiCoP heterostructure on N-doped carbon for highly efficient and pH-universal hydrogen evolution electrocatalysis[J]. Adv. Funct. Mater., 2019, 29(6): 1807976.

[46] Du Y M, Qu H Q, Liu Y R, Han Y, Wang L, Dong B. Bimetallic CoFeP hollow microspheres as highly efficient bifunctional electrocatalysts for overall water splitting in alkaline media[J]. Appl. Surf. Sci., 2019, 465: 816-823.

[47] Cui L, Sun X P, Xu Y H, Yang W R, Liu J Q. Cobalt carbonate hydroxide nanowire array on Ti mesh: an efficient and robust 3D catalyst for on-demand hydrogen generation from alkaline $NaBH_4$ solution[J]. Chem. Eur.J., 2016, 22(42): 14831-14835.

[48] Zhang Y X, Xiao Q Q, Guo X, Zhang X X, Xue Y F, Jing L, Zhai X, Yan Y M, Sun K N. A novel electrocatalyst for oxygen evolution reaction based on rational anchoring of cobalt carbonate hydroxide hydrate on multiwall carbon nanotubes[J]. J. Power Sources, 2015, 278: 464-472.

[49] Veerasubramani G K, Chandrasekhar A, P. Sudhakaran M S P, Mok Y S, Kim S J. Liquid electrolyte mediated flexible pouch-type hybrid supercapacitor based on binderless core-shell nanostructures assembled with honeycomblike porous carbon[J]. J. Mater. Chem. A, 2017, 5 (22): 11100-11113.

[50] Lu X Y, Zhao C A. Electrodeposition of hierarchically structured three-dimensional nickel-iron electrodes for efficient oxygen evolution at high current densities[J]. Nat. Commun., 2015, 6: 6616.

[51] Bates M K, Jia Q Y, Doan H, Liang W T, Mukerjee S. Charge-transfer effects in Ni-Fe and Ni-Fe-Co mixed-metal oxides for the alkaline oxygen evolution reaction [J]. ACS Catal., 2016, 6(1): 155-161.

[52] Louie M W, Bell A T. An investigation of thin-film Ni-Fe oxide catalysts for the electrochemical evolution of oxygen[J]. J. Am. Chem. Soc., 2013, 135(33): 12329-12337.

[53] Zhou Q W, Pu J, Sun X L, Zhu C, Li J C, Wang J, Chang S Z, Zhang H G. *In situ* surface engineering of nickel inverse opal for enhanced overall electrocatalytic water splitting[J]. J. Mater. Chem. A, 2017, 5(28): 14873-14880.

[54] Feng J X, Xu H, Dong Y T, Ye S H, Tong Y X, Li G R. FeOOH/Co/FeOOH hybrid nanotube arrays as high-performance electrocatalysts for the oxygen evolution reaction[J]. Angew. Chem. Int. Ed., 2016, 55(11): 3694-3698.

[55] Yang Y, Kang Y K, Zhao H H, Dai X P, Cui M L, Luan X B, Zhang X, Nie F, Ren Z T, Song W Y. An interfacial electron transfer on tetrahedral $NiS_2/NiSe_2$ heterocages with dual-phase synergy for efficiently triggering the oxygen evolution reaction[J]. Small, 2020, 16(1): 1905083.

[56] Xia J L, Zhao H Y, Huang B L, Xu L L, Luo M, Wang J W, Luo F, Du Y P, Yan C H. Efficient optimization of electron/oxygen pathway by constructing ceria/hydroxide interface for highly active oxygen evolution reaction[J]. Adv. Funct. Mater., 2020, 30(9): 1908367.

[57] Lei Z W, Bai J J, Li Y B, Wang Z L, Zhao C. Fabrication of nanoporous nickel-iron hydroxyl phosphate composite as bifunctional and reversible catalyst for highly efficient intermittent water splitting[J]. ACS Appl. Mater. Interfaces, 2017, 9(41): 35837-35846.

[58] Song B, Li K, Yin Y, Wu T, Dang L N, Caban-Acevedo M, Han J C, Gao T L, Wang X J, Zhang Z H, Schmidt J R, Xu P, Jin S. Tuning mixed nickel iron phosphosulfide nanosheet electrocatalysts for enhanced hydrogen and oxygen evolution[J]. ACS Catal., 2017, 7(12): 8549-8557.

[59] Wang J Y, Wang J, Zhang M, Li S M, Liu R, Li Z Q. Metal-organic frameworks-derived hollow-structured iron-cobalt bimetallic phosphide electrocatalysts for efficient oxygen evolution reaction[J]. J. Alloys Compd., 2020, 821: 153463.

[60] Wu H, Lu X, Zheng G F, Ho G W. Topotactic engineering of ultrathin 2D nonlayered nickel selenides for full water electrolysis[J]. Adv. Energy Mater., 2018, 8(14): 1702704.

[61] Zhang P L, Li L, Nordlund D, Chen H, Fan L Z, Zhang B B, Sheng X, Daniel Q, Sun L C. Dendritic core-shell

nickel-iron-copper metal/metal oxide electrode for efficient electrocatalytic water oxidation[J]. Nat. Commun., 2018, 9: 381.

[62] Yu M Z, Wang Z Y, Liu J S, Sun F, Yang P J, Qiu J S. A hierarchically porous and hydrophilic 3D nickel-iron/mxene electrode for accelerating oxygen and hydrogen evolution at high current densities[J]. Nano Energy, 2019, 63: 103880.

[63] Song F, Hu X L. Exfoliation of layered double hydroxides for enhanced oxygen evolution catalysis[J]. Nat. Commun., 2014, 5: 4477.

[64] Zhu X L, Tang C, Wang H F, Zhang Q, Yang C H, Wei F. Dual-sized NiFe layered double hydroxides *in situ* grown on oxygen-decorated self-dispersal nanocarbon as enhanced water oxidation catalysts[J]. J. Mater. Chem. A, 2015, 3(48): 24540-24546.

[65] Park Y S, Yang J C, Lee J M, Jang M J, Jeong J, Choi W S, Kim Y, Yin Y D, Seo M H, Chen Z W, Choi S M. Superior performance of anion exchange membrane water electrolyzer: ensemble of producing oxygen vacancies and controlling mass transfer resistance[J]. Appl. Catal. B, 2020, 278: 119276.

自支撑 NiFe LDHs@Co-OH-CO_3 纳米棒阵列电极用于碱性阴离子交换膜电解水

郭丹丹[1,2],俞红梅[1*],迟 军[1],邵志刚[1*]

(1. 中国科学院大连化学物理研究所, 辽宁 大连 116023; 2. 中国科学院大学,北京 100049)

摘要: 开发高效耐用的电极对碱性阴离子交换膜电解水(AEMWEs)制氢至关重要。在这项研究中,我们展示了一种高效且稳定的自支撑 NiFe LDHs@Co-OH-CO_3/NF 纳米棒阵列电极分别用于析氧反应(OER)和 AEMWE 的阳极。在这项工作中,我们将 2D 的镍铁层状双金属氢氧化物纳米片(NiFe LDHs)原位生长在 1D 的碱式碳酸钴纳米线上(Co-OH-CO_3/NF),最终得到独特的纳米棒阵列复合结构电极。在三电极体系中,自支撑 NiFe LDHs@Co-OH-CO_3/NF 对 OER 具有良好的催化活性, 在 1 mol·L^{-1} KOH 中, 当电流密度为 20 mA·cm^{-2} 时, 过电位为 215 mV。当自支撑 NiFe LDHs@Co-OH-CO_3/NF 作为 AEMWE 的阳极(70 ℃, 1 mol·L^{-1} KOH),在电流密度为 0.5 A·cm^{-2} 时, 电解电压为 1.72 V, 并且具有较好的稳定性。进一步的实验表征结果显示了自支撑 NiFe LDHs@Co-OH-CO_3/NF 的优异性能是其具有特殊的形貌结构。这是由于纳米棒阵列电极的三维分层结构可以有效防止纳米片团聚, 从而有利于电子转移,为水分解提供大量的边缘活性位点。

关键词: 镍铁层状双金属氢氧化物;析氧反应;碱性阴离子交换膜电解